2016

Behavior of large-scale hybrid FRP-concrete-steel double-skin tubular beams with shear connectors

J L. Zhao
The Hong Kong Polytechnic University

Jin Guang Teng
The Hong Kong Polytechnic University, cejgteng@polyu.edu.hk

Tao Yu
University of Wollongong, taoy@uow.edu.au

L J. Li
University of Technology, Guangzhou

Behavior of large-scale hybrid FRP-concrete-steel double-skin tubular beams with shear connectors

Abstract

Hybrid fiber-reinforced polymer (FRP)-concrete-steel double-skin tubular members (DSTMs) are a new form of hybrid members that consist of an outer tube made of FRP and an inner tube made of steel, with the space between them filled with concrete. The existing studies on hybrid DSTMs have been mainly focused on their use as compression members, with only a very limited number of studies on their use as flexural members [i.e., hybrid double-skin tubular beams (DSTBs)]. This paper presents the first ever experimental study on large-scale hybrid DSTBs with headed shear studs; the effect of an integrated deck is also examined. The main parameter examined in the experimental program was the section configuration. The test results show that both the DSTBs and the DSTB-deck unit possessed a very ductile response, and that the headed shear studs effectively reduced or eliminated slips between the steel tube and the concrete. This paper also presents a theoretical model based on conventional section analysis. The predictions from the theoretical model are in reasonably close agreement with the test results.

Disciplines

Engineering | Science and Technology Studies

Publication Details

Zhao, J. L., Teng, J. G., Yu, T. & Li, L. J. (2016). Behavior of large-scale hybrid FRP-concrete-steel double-skin tubular beams with shear connectors. Journal of Composites for Construction, 20 (5), 04016015-1-04016015-11.

BEHAVIOR OF LARGE-SCALE HYBRID FRP-CONCRETE-STEEL DOUBLE-SKIN TUBULAR BEAMS WITH SHEAR CONNECTORS

J.L. Zhao[1], J.G. Teng[2,*], T. Yu[3] and L.J. Li[4]

ABSTRACT

Hybrid FRP-concrete-steel double-skin tubular members (DSTMs) are a new form of hybrid members which consist of an outer tube made of FRP and an inner tube made of steel, with the space between them filled with concrete. The existing studies on hybrid DSTMs have been mainly focused on their use as compression members, with only a very limited number of studies on their use as flexural members (i.e. hybrid double-skin tubular beams or DSTBs). This paper presents the first ever experimental study on large-scale hybrid DSTBs with headed shear studs; the effect of an integrated deck is also examined. The main parameter examined in the experimental program was the section configuration. The test results show that both the DSTBs and the DSTB/deck unit possessed a very ductile response, and that the headed shear studs effectively reduced/eliminated slips between the steel tube and the concrete. This paper also presents a theoretical model based on conventional section analysis. The predictions from the theoretical model are in reasonably close agreement with the test results.

KEWWORDS

FRP tubes; Hybrid members; Tubular members; Beams; Shear connectors; Large-scale tests

[1] PhD Candidate, Department of Civil and Environmental Engineering, The Hong Kong Polytechnic University, Hong Kong, China.
[2] Chair Professor of Structural Engineering, Department of Civil and Environmental Engineering, The Hong Kong Polytechnic University, Hong Kong, China (Corresponding author). Email address: cejgteng@polyu.edu.hk; Fax: +852-2334-6389; Tel: +852-2766-6012.
[3] Senior Lecturer, School of Civil, Mining and Environmental Engineering, Faculty of Engineering and Information Sciences, University of Wollongong, NSW, Australia.
[4] Professor, School of Civil and Transportation Engineering, Guangdong University of Technology, Guangzhou, China.

INTRODUCTION

Over the past two decades, fiber-reinforced polymer (FRP) has emerged as a popular structural material to strengthen/retrofit existing structures (Teng et al. 2002; Hollaway and Teng 2008; Teng et al. 2012). The success of FRP composites in the strengthening of structures has also led to many studies exploring their potential in the construction of new structures (e.g. Fam and Rizkalla 2001; Mirmiran 2003; Kim et al. 2009; Li et al. 2013), where the combined use of FRP with other materials to create hybrid structures is a very promising direction (Mirmiran 2003; Teng et al. 2007).

Hybrid FRP-concrete-steel double-skin tubular members (DSTMs) (Figs. 1 and 2) are a new form of hybrid members developed at The Hong Kong Polytechnic University (Teng et al. 2004, 2007). A hybrid DSTM consists of an outer tube made of FRP and an inner tube made of steel, with the space between them filled with concrete. The two tubes may be concentrically placed (Fig. 1) to produce a section form more suitable for columns, or eccentrically placed for use in beams (Fig. 2). This paper is concerned with flexural members of such hybrid sections (referred to as hybrid double-skin tubular beams or hybrid DSTBs for brevity) where the inner steel tube is typically shifted towards the tension side. In hybrid DSTBs, the FRP outer tube offers mechanical resistance primarily in the hoop direction to confine the concrete and to enhance the shear resistance of the beam. Such FRP tubes can be manufactured by filament winding with fibers oriented close to the hoop direction. Hybrid DSTBs may be constructed in-situ or precast, with the two tubes acting as the stay-in-place form. The sections of the two tubes may be both circular (Fig. 2a), rectangular (Fig. 2c), or in another shape; they may also have shapes different from each other (Fig. 2b). As bridge girders, hybrid DSTBs can be used with an all FRP deck (or a hybrid FRP-concrete deck) to form a light slab-on-girder bridge system. They can also be integrated into a concrete deck reinforced with FRP bars to form a corrosion-resistant bridge system (Fig. 3).

47 Shear connectors are needed between the steel tube and the concrete (Yu et al. 2006; Liu
48 and Qian 2007; Wang and Tao 2009; Idris and Ozbakkaloglu 2014) but not needed for the
49 FRP tube, which has a small longitudinal stiffness/resistance and can develop sufficient
50 interaction with concrete through the normal pressure and interfacial friction between the
51 confining FRP tube and the concrete. The shear connectors on the lower part of the steel tube
52 also act as positioning spacers between the FRP tube and the steel tube (Fig. 2).

53 The greatest advantage of hybrid DSTBs is their excellent corrosion resistance, as the
54 FRP tube is highly resistant to corrosion while the steel tube is protected by the FRP tube and
55 the concrete and if necessary by sealing the ends of the steel tube with welded steel plates.
56 The other main advantages of hybrid DSTBs include: (1) excellent ductility, as the steel tube
57 acts as ductile longitudinal reinforcement and the concrete is well confined by the two tubes;
58 (2) light weight as the inner void largely eliminates the redundant tensile concrete; (3) ease for
59 construction, as the two tubes act as a permanent form for casting concrete, and the presence
60 of the inner steel tube and concrete allows easy connection to other members. In addition, the
61 steel tube ensures a large flexural stiffness of the hybrid DSTB, which eliminates a major
62 deficiency of concrete beams reinforced with FRP bars, where excessive deflections instead
63 of strength become a controlling criterion due to the relatively low elastic modulus of FRP
64 bars (Abdalla 2002).

65 A large amount of research has been conducted on hybrid DSTMs since its invention. The
66 existing studies have been mainly focused on the behavior of hybrid double-skin tubular
67 columns (DSTCs), including the behavior of columns under concentric and eccentric axial
68 compression (Yu 2007; Qian and Liu 2006, 2008a, b; Teng et al. 2007; Wong et al. 2008; Yu
69 et al. 2010a, b; Yu et al. 2012; Yu and Teng 2013; Ozbakkaloglu and Fanggi 2014) and under
70 combined axial compression and cyclic lateral loading (Qian and Liu 2008c; Han et al. 2010;
71 Ozbakkaloglu and Idris 2014; Zhang et al. 2015), as well as finite element modelling (Yu et al.

2010c, d). To the best of the authors' knowledge, only four studies (i.e. Yu et al. 2006; Liu and Qian 2007; Wang and Tao 2009; Idris and Ozbakkaloglu 2014) have been published on hybrid DSTBs. The flexural tests presented in these studies have generally confirmed that hybrid DSTBs possess a very ductile response as the FRP tube confines the concrete and provides additional shear resistance while the steel tube provides ductile longitudinal reinforcement. These flexural tests have also revealed that significant slips between the concrete and the steel tube may occur which can cause reductions/fluctuations in load resistance, pointing to the need for appropriate shear connectors between them. The existing studies on hybrid DSTBs, however, have been limited to the testing of small-scale specimens, with the outer diameter/side length of specimens being less than 200 mm. These studies have also been generally limited to specimens without shear connectors between the steel tube and the concrete; only a single specimen tested by Idris and Ozbakkaloglu (2014) used welded steel rings as shear connectors. Against this background, this paper presents the results of a recent experimental study where large-scale hybrid DSTBs with headed shear studs were tested. Headed shear studs were used because of their ease for installation and wide acceptance by the construction community (Johnson 1994; Oehlers and Bradford 1999; Collings 2005; Nie 2011). These stand-alone DSTBs represent practical situations where the bridge deck is not integrated with the girders or the deck does not possess a substantial compressive resistance (e.g. a lightweight FRP bridge deck). The experimental program also included the testing of a hybrid DSTB/deck unit (Fig. 3); such units have not previously been studied. Results from theoretical modeling are also presented and compared with the test results.

EXPERIMENTAL PROGRAM

Test Specimens

A total of four large-scale specimens were prepared and tested, including three hybrid DSTBs and one DSTB/deck unit. All the specimens had an overall length of 5 m. Three different

cross-sectional configurations were adopted for the three DSTB specimens respectively, with the main difference being the shapes of the two tubes (i.e. FRP outer tube and steel inner tube). The DSTB/deck unit specimen consisted of a DSTB integrated into a concrete deck reinforced with basalt FRP (BFRP) bars. Details of the four specimens are shown in Figs. 2 and 3. Each specimen was given a name, which starts with a letter "R" or "C" to represent the shape (i.e. rectangular or circular) of the FRP outer tube, followed by another letter ("R" or "C") to represent the shape of the steel inner tube. The last letter "U" in one of the specimens is used to indicate that this is a DSTB/deck unit.

All the FRP tubes were custom-made filament-wound tubes. The circular FRP tubes used in specimens CC and CCU both had an inner diameter of 500 mm and a thickness of 3.63 mm. The rectangular FRP tubes used in specimens RC and RR both had a height of 480 mm, but they had a width of 400 mm for specimen RC and 300 mm for specimen RR. When producing the rectangular FRP tubes, a rectangular wooden mold formed from four wooden panels was used, in which four circular fillets were used at the four corners respectively to achieve a corner inner radius of 30 mm. The circular steel tubes in specimens CC, RC and CCU were hot-rolled seamless tubes from the same batch, with an outer diameter of 325 mm and a thickness of 7.2 mm. The rectangular steel tube in specimen RR was a cold-formed steel tube with an outer width of 250 mm, an outer height of 350 mm and a thickness of 9.2 mm. In all the specimens, the steel inner tube was shifted to the tension side of the cross-section for improved flexural performance (Figs. 2 and 3). The minimum thickness of concrete layer on the tension side was 30 mm for all the specimens (Figs. 2 and 3). The cross-sections of the specimens were chosen based on the following considerations: (a) a sufficiently large void ratio to significantly reduce the weight/amount of concrete of the beam (the void area was generally larger than 40% of the area enclosed by the FRP tube); (b) ready availability of steel tubes and FRP tubes in the market; (c) preference for thinner tubes to cut the material cost as

122 the tubes in the market tended to be thicker than was needed to achieve good mechanical
123 behavior; (d) full-height shear studs could be installed on the compression side of the steel
124 tube.

125 Headed shear studs were welded onto the surface of the inner steel tube (Figs. 2 and 3).
126 The shear studs were designed to be sufficient for load transfer between the concrete and the
127 steel tube based on a rigid plastic analysis (Oehlers and Bradford 1999), where all materials
128 are assumed to be fully yielded and possess unlimited ductility. Three groups of shear studs,
129 being 45º apart from each other, were welded on the compression side of each circular steel
130 tube in specimens RC, CC and CCU (Figs. 2a, b and 3); each group consisted of a number of
131 studs located at a longitudinal spacing of 120 mm (for specimens RC and CC) or 100 mm (for
132 specimen CCU). For specimen RR, two groups of studs were welded on the top side of the
133 rectangular steel tube; the studs in each group were at a longitudinal spacing of 120 mm. All
134 the shear studs had a diameter of 16 mm and a height of 95 mm after welding. Besides the
135 studs on the compression side of the steel tubes, shorter studs were also welded on the lower
136 part of the steel tubes as positioning spacers.

137 In specimen CCU, a BFRP-reinforced concrete deck was integrated with a DSTB,
138 leading to a hybrid section with a height of 570 mm (Fig. 3). Two layers of off-the-shelf
139 sand-coated BFRP bars were provided in the deck, where each layer consisted of bars in both
140 the longitudinal and the transverse directions. Following ASTM D7205 (2006), the nominal
141 cross-sectional area of the FRP bars used in the present study was determined to be 126 mm^2,
142 so the corresponding effective diameter is 12.7 mm. The spacing of bars in both directions
143 was 100 mm, except that no longitudinal bars were provided within the FRP tube (Fig. 3). The
144 bottom layer of transverse BFRP bars passed through the FRP tube and served also as
145 mechanical connectors between the concrete deck and the DSTB. The net thickness of
146 concrete cover in the deck was 15 mm. The BFRP bars were designed according to ACI

147 440.1R (2006) to ensure that failure of the deck would be initiated by concrete crushing (i.e.
148 $\rho_f > 1.4\rho_{fb}$, where ρ_f and ρ_{fb} are the reinforcement ratio and the balanced reinforcement
149 ratio respectively). In addition, U-shaped stainless steel bars, with a diameter of 20 mm and at
150 a longitudinal spacing of 200 mm, were provided to enhance composite action in the
151 beam/deck unit (Fig. 3).

152 The preparation process of a DSTB specimen included the following steps: (1)
153 preparation of the steel tube, which included cutting the tube to a desired length, removing the
154 rust at the positions of shear studs and welding of shear studs to the steel tube using an
155 automatic arc stud welding machine following BS/EN/ISO 14555 (2006); (2) turning the steel
156 tube to the vertical position and fixing it to a strong wall; (3) placing the FRP tube outside the
157 steel tube; (4) casting self-compacting concrete (SCC) between the two tubes; and (5) turning
158 the specimen to the horizontal position and leaving it to cure at room temperature for about
159 seven months before testing. For the DSTB/deck unit, the preparation process included all the
160 steps listed above and the following additional steps between (3) and (4): preparing the BFRP
161 cage and a wooden form for casting the concrete deck. It should be mentioned that, in real
162 applications, DSTBs can be cast in the horizontal position using a concrete pump.

163

164 ***Material Properties***

165 All the specimens were cast using the same batch of ready-mix, self-compacting concrete.
166 High strength concrete with a target compressive strength of 60 MPa was used as normal
167 strength SCC was not available to the authors. The adoption of high strength concrete is
168 believed to have no significant effect on the mechanisms of behavior of the DSTBs based on
169 previous studies (Yu et al. 2006; Idris and Ozbakkaloglu 2014). Three standard concrete
170 cylinders (150 mm × 300 mm) were prepared and tested according to ASTM C-469 (2002)
171 around the time of the testing the beams. The elastic modulus (E_c), compressive strength (f'_{co})

and compressive strain (ε_{co}) at peak stress of the concrete averaged from the concrete cylinder tests were 31.1 GPa, 69.0 MPa and 0.287% respectively.

Tensile tests were conducted to determine the material properties of steel tubes, stainless steel bars and headed shear studs following BS18 (1987). These included tests on: (1) five coupons cut from the two 12-m long circular steel tubes (two from one and three from the other steel tube) of the same batch used in the experimental program; (2) six coupons from the rectangular steel tube, including three cut from the webs and three from regions close to the corners; (3) three stainless bar specimens; and (4) two shear studs, which were machined to dog-bone shaped specimens. From the coupon tests, the stress-strain curves of steel close to the corners of the rectangular tube are significantly different from those of steel from the webs, with the former having a significantly higher strength and no apparent plastic plateau. This is believed to be due to the cold forming process of making the rectangular tube. The average elastic modulus, yield stress and tensile strength obtained from these tests are summarized in Table 1, where the elastic moduli were calculated using strains measured by two strain gauges attached on the two sides of each specimen. For the rectangular steel tube, two sets of values are provided, which were averaged from the web coupon tests and the corner coupon tests respectively. The elastic modulus and tensile strength of BFRP bars from the manufacturer are also provided in Table 1.

Two types of FRP tubes were used in the present study, which were both produced via a filament-winding process using E-glass fibers and vinyl ester resin. The number of layers of all FRP tubes was 8. The mechanical properties of the fiber and the resin as provided by the manufacturer are summarized in Table 2. The circular tubes had an actual thickness of 3.63 mm. The nominal fiber volume ratio was 0.51, based on the nominal fiber thickness (i.e. 1.85 mm) provided by the manufacturer. The fibers were oriented at ±84º with respect to the longitudinal axis of the tube. The fibers in the rectangular FRP tubes were also oriented at

±84º to the longitudinal axis, but the actual thickness of the tubes varied around the perimeter. The variation in thickness was mainly due to the uneven distribution of resin around the perimeter, with less resin in corner regions than mid-side regions, as a result of the fabrication process; this thickness variation is expected to have only a small effect on the mechanical properties of the tube as the amount of fibers was constant over the tube. Six coupons were cut from each of the two rectangular tubes in the hoop direction and were tested following ASTM D3039 (2008), whose test apparatus and procedure are the same as those specified by ASTM D7565 (2010). The elastic modulus, tensile strength and rupture strain averaged from these tests were 85.0 GPa, 1595 MPa and 1.90% respectively for specimen RC, and were 78.8 GPa, 1543 MPa and 1.98% respectively for specimen RR, all based on a nominal thickness of 1.85 mm. The hoop properties of circular FRP tubes were not tested due to the difficulty in conducting splitting disk test on such a large tube. However, the hoop properties of the circular FRP tubes are expected to be similar to those of the rectangular FRP tubes, as they had the same amount of fibers and the same winding angle.

Test Set-Up and Instrumentation

The three DSTBs were tested under four-point bending while the DSTB/deck unit was tested under three-point bending. The two ends of the beams were simply supported, and the steel tubes near the supports were left hollow. The test set-up is shown in Fig. 4.

Extensive strain gauging and many linear variable displacement transducers (LVDTs) were employed to monitor the behavior of the specimens. The LVDTs were used to measure in-span deflections, support settlements, and interfacial slips of the tubes against the concrete. Three cross-sections, namely Sections A, B and C, were installed with many strain gauges on the steel tube and the FRP tube in both the hoop and the longitudinal directions. The layout of the strain gauges is shown in Fig. 4c.

All the tests were carried out using a loading frame with one (for three-point bending) or two MTS actuators (for four-point bending). Displacement control was adopted for all the tests with a rate of 1.5 mm/min. Fig. 5 shows tests in progress. For the four-point bending tests, one of the two actuators served as the control actuator, whose output force was used as the input of the other actuator so that the loads applied by both actuators were always the same. All test data, including the strains, loads, and displacements, were recorded simultaneously by a data logger.

TEST RESULTS AND DISCUSSIONS

General Observations

All the tests were terminated due to the limit of space between the test beam and the laboratory floor; no apparent reduction in the load carried by the beam was noted at the end of test in all four cases. It is also believed that the load that could be carried by the specimens would not increase significantly afterwards as the steel tube had almost fully yielded at test termination. Therefore, the load at test termination can be taken as the ultimate load. The four specimens after test are shown in Fig. 6, where it is evident that the specimens were generally in a good state except for a number of cracks on the tension side of the FRP tube. The tensile cracks were generally more uniformly distributed between the two loading points than elsewhere for specimens under four-point bending (i.e. specimens CC, RC and RR). For specimen CCU which was under three-point bending, the tensile cracks were localized near the mid-span. As a result, the deflections were also more localized near the mid-span for specimen CCU, as shown in Fig. 7, where the deflected shapes of both CC and CCU are shown. In Fig. 7, the horizontal axis represents the distance to the left support and the deflections were obtained from the LVDTs installed at different locations (see Fig. 4 for details).

Further examination of the tested specimens revealed that local buckling of the FRP tube occurred on the compression side of specimens RC and RR, which both had a rectangular FRP tube (Fig. 6), but did not occur in the circular FRP tubes of the other two specimens. For specimen CCU, slight crushing of concrete was observed on the top surface of the deck at the mid-span (i.e. line of loading); tensile cracks were also noted on the bottom surface of the deck, suggesting that the neutral axis was within the concrete deck. Readings from LVDT 11 (see Fig. 4) revealed that the relative deformation between the top and bottom of the steel tubes due to the bearing force at the support was very small (i.e. < 1mm) for all the specimens.

Load-Deflection Behavior

The load-deflection curves of all the specimens are shown in Fig. 8. The load P shown in Fig. 8 represents the average load output of the two actuators for the specimens under four-point bending, and half of the load output of the single actuator in the three-point bending test (see also Fig. 4). The deflection shown in Fig. 8 is the mid-span deflection of the specimens, and was obtained by excluding the effect of the support settlements. The mid-span deflections were from LVDT 3 for specimens CC, RC and RR, and averaged from LVDTs 3, 12 and 13 for specimen CCU (see Fig. 4).

It is evident from Fig. 8 that all the specimens generally exhibited a smooth load-deflection curve except for specimen RR, where a small load drop was observed at a mid-span deflection of about 130 mm. The small load drop was due to the sudden appearance of a tensile crack on the FRP tube; afterwards the specimen could still be reloaded to exceed the original load level. All the curves of the three DSTB specimens have an approximately flat second branch, while that of the beam/deck unit (i.e. specimen CCU) possesses a slightly ascending second branch. The maximum deflections shown in Fig. 8 are the deflections at the

termination of the test due to the space limit of the loading frame, so they do not represent the ultimate state of the specimen. The ductility of the specimens can be expected to be significantly larger than is indicated by Fig. 8.

The moment-strain curves of all the specimens are shown in Fig. 9, where the moments are those at the mid-span and were calculated from the applied loads, while the strains are those at the extreme compression fiber of the mid-span section and were obtained from strain gauge readings (i.e. from the strain gauge attached at the top of FRP tube for specimens CC, RC and RR, and from that attached at the top of the deck for specimen CCU).

Cracking of FRP Tube

Cracking of the FRP tube due to tensile stresses in the longitude direction was found in all four tests at a load significantly below the ultimate load; this cracking was generally along one of the fiber directions on the bottom part of the FRP tube. In the specimens under four-point bending (i.e. specimens CC, RC and RR), the first crack occurred within the constant moment region; in specimen CCU, which was subjected to three-point bending, the first crack was very close to the mid-span. The development of cracks can also be identified from the readings of strain gauges. Fig. 10 shows a typical compressive-tensile strain curve for specimen CC, where the compressive and tensile strains are from two strain gauges located at the top and bottom of the mid-span section respectively (i.e. section B in Fig. 4). In this paper, tensile strains are defined to be negative while compressive strains are defined to be positive. In Fig. 10, the curve is seen to be initially smooth until point A when the first crack occurred at around 400 mm from the mid-span (Fig. 11a); the occurrence of the crack led to a sudden release of tensile stress at that point and consequently a sudden decrease of tensile strain measured at the mid-span (Fig. 10). Similarly, the cracks shown in Figures 11b~d led to the sudden decreases of the tensile strain corresponding to points B~D of Figure

297 10. Finally, the tensile strain remained to be small because of the occurrence of a crack which
298 was very close to the mid-span (Fig. 11d). The development of cracks as shown in Figs. 10
299 and 11 also suggests that the cracking strain was around 0.15%, which is consistent with the
300 observations from other specimens.

301 The loads at the first cracking of FRP tubes were 58%, 69% and 83% of the
302 corresponding ultimate loads for specimens CC, RC and RR respectively. These loads are
303 generally high than the service load to be expected on a bridge girder. For specimen CCU, the
304 first-cracking load was only 20% of its ultimate load; for such a specimen, the first cracking
305 load needs to be enhanced to avoid the cracking of the FRP tube under service to ensure that
306 the FRP tube can protect the steel tube from corrosion. This enhancement can be achieved by
307 orienting the fibers at a smaller angle to the longitudinal direction. Therefore, optimization of
308 fiber orientations in the FRP tube, to provide good confinement as well as a desirable level of
309 resistance to cracking, is a topic that needs further research.

310

311 ***Development of Strains***

312 Longitudinal Strains

313 The readings of longitudinal strain gauges installed on section A (Fig. 4) are shown against
314 the load P in Figs. 12a~12c for specimens CC, RC and RR respectively. The curves for
315 specimen CCU are not shown as some of the strain gauges were damaged during the test. The
316 group of curves shown on the left in these figures was from the strain gauges on the steel tube;
317 the group shown on the right was from the strain gauges on the FRP tube. Among each group
318 of curves, those on the right side (i.e. positive strains) were from the strain gauges on the
319 upper part of the section while those on the left side (i.e. negative strains) were from the lower
320 strain gauges. The left groups of curves are generally linear until the end of the test, indicating
321 that the steel tube did not yield at section A during the test. The right groups of curves are also

initially linear before the cracking of FRP tube, which is signified by a sudden decease of strain on the leftmost curves.

Fig. 12d shows the distribution of longitudinal strains down the section height at a load which is slightly lower than that at the first cracking of FRP tube. It is evident that the strain distributions for specimens CC and RC generally followed the plane section assumption, with the strains of the steel tube being very similar or identical to those of the FRP tube at the same height, suggesting that the slip between the concrete and the steel tube was minimal. For specimen RR, the strain distributions in the two tubes show noticeable differences, indicating the existence of some small slips between the steel tube and the concrete in this specimen.

Hoop Strains

The development of hoop strains during the deformation process is shown in Fig. 13, where the hoop strains are those measured at the mid-span section by a number of strain gauges installed on the FRP tube. The mid-span load-deflection curves, as well as the layout of strain gauges, are also shown in Fig. 13 for reference. It is evident from Fig. 13 that the hoop strains were generally very small during the elastic range (i.e. the first branch of the load-deflection curve), suggesting that the FRP tube was not yet activated. The largest hoop strain generally occurred at or close to the top of the FRP tube (i.e. extreme compression zone), except for specimen CCU where the expansion of the upper part of FRP tube was restrained by the concrete deck. At the end of test, the maximum measured hoop strains over the FRP tube section were 0.73%, 0.42%, 0.26% and 0.24% respectively for the four specimens, which are all well below the rupture strain of the FRP tube, suggesting that the specimens may have a much larger deflection capacity than those recorded in the tests.

Relative Slips between the Concrete and the Tubes

The development of relative slips between the inner steel tube and the concrete at the two ends is shown in Fig. 14 for each specimen. The slips were measured using LVDTs 8 and 9 (Fig. 4). It is evident that the slips were generally very small, with the largest value being only 0.22 mm, measured in specimen CCU. For a DSTB without shear connectors, Idris and Ozbakkaloglu (2014) reported a much larger slip (i.e. 9 mm) for a specimen of a much smaller scale (i.e. span length = 1300 mm). Idris and Ozbakkaloglu (2014) showed that substantial slips had developed before the attainment of the peak load of their beams, but the slips in the present tests remained to be very small even at the peak load. The shear studs used in the present study was therefore very effective in ensuring a high degree of composite action between the steel and the concrete.

The development of relative slips between the FRP tube and the concrete is shown in Fig. 15, where the slips were measured by LVDT 10 (see Fig. 4). The slips were also very small, with the maximum value being less than 1 mm.

THEORETICAL ANALYSIS

A traditional section analysis was developed for the hybrid DSTBs and the DSTB/deck unit following Yu *et al.* (2006). The following assumptions are adopted in the section analysis: (1) plane sections remain plane; and (2) the contribution of FRP tube in the longitudinal direction is small and can be ignored. The analytical procedure involves the determination of the neural axis position for a given strain of the extreme compression fiber by force equilibrium and the evaluation of the bending moment by integrating the contributions of stresses over the section.

The average stress-strain curves from the coupon tests are adopted for the steel tubes. A linear elastic stress-strain curve is adopted for the BFRP bars in specimen CCU with the elastic modulus and tensile strength being those given by the manufacturer (see Table 1). The diameter of the BFRP bars was taken as 12 mm in the analysis, on which the mechanical

properties provided by the manufacturer were based. The following stress-strain relationship is adopted for the concrete in compression:

$$\sigma_c = \begin{cases} f'_{co}\left[\dfrac{2\varepsilon_c}{\varepsilon_{co}} - \left(\dfrac{\varepsilon_c}{\varepsilon_{co}}\right)^2\right] & 0 \le \varepsilon_c \le \varepsilon_{co} \\ f'_{co} & \varepsilon_{co} < \varepsilon_c \quad \text{confined} \\ f'_{co}\left(1 - 0.15\dfrac{\varepsilon_c - \varepsilon_{co}}{\varepsilon_{cu} - \varepsilon_{co}}\right) & \varepsilon_{co} < \varepsilon_c < \varepsilon_{cu} \quad \text{unconfined} \end{cases} \tag{1}$$

where f'_{co} is taken as 0.85 times the unconfined concrete strength from the cylinder tests; ε_{co} is the strain at f'_{co}; ε_{cu} is the ultimate axial strain of unconfined concrete taken as 0.0038 following Hognestad (1951). The concrete in the DSTBs is treated as confined concrete while the concrete in the deck of the DSTB/deck unit is treated as unconfined concrete. Eq. (1) only accounts for the increase in strain capacity due to confinement but ignores any enhancement in the ultimate stress due to confinement, which is a conservative approximation of the confinement effect in a flexural member.

Both the confined and unconfined concretes are assumed to behave linear-elastically in tension with the elastic modulus being the same as that in compression, until the tensile stress reach the tensile strength of concrete defined by CEB-FIP (1993):

$$f_t = 1.4\left(\frac{f'_{co}}{10}\right)^{2/3} \tag{2}$$

The tensile stress in concrete is assumed to reduce to zero immediately when the tensile strength is reached.

Moment-Strain Curves

In the section analyses of the present study, the height of each horizontal layer was chosen to be 5 mm for the three DSTBs (i.e. specimens CC, RC and RR) and 1 mm for specimen CCU based on a convergence study. The section analyses were terminated when the strain of extreme compression fiber of concrete reached the maximum compressive strain on the FRP

393 tube section measured at the end of the test.

394 The predicted moment-compressive strain curves are compared with the test results in Fig.
395 16, where the strains are those of the extreme compression fiber. The loads carried by the
396 three DSTBs (i.e. specimens CC, RC and RR) are a little overestimated at large strain levels.
397

398 ***Load-Deflection Curves***

399 Once the moment-curvature curves are available, the load-deflection curves can be predicted
400 by integration (De Silva 2014). The predicted mid-span load-deflection curves are compared
401 with the test results in Fig. 17, where the predicted curves terminate at their respective
402 maximum deflections recorded in the tests. In Fig. 17, the predictions agree reasonably well
403 with the test results for specimens CC, RC and RR, except that the loads carried by the
404 DSTBs are slightly overestimated at large deflection levels. This overestimation may be
405 attributed to possible slips between the steel tube and the concrete, which may be significant
406 larger within the span than those measured at the beam end (Gattesco 1999). For specimen
407 CCU, however, the predictions significantly overestimate the stiffness of the specimen and the
408 load resisted by the beam during the second ascending stage. This can be attributed to the
409 slips between the DSTB and the concrete deck due to insufficient shear connections between
410 the two; unfortunately, these slips were not measured during the test. Further research is
411 therefore needed to establish a more effective measure to ensure full composite action in a
412 DSTB/deck unit.

413 The predicted deflections at different load levels are compared with the test results of
414 specimen CC and CCU in Fig. 7; the comparisons for the other two DSTB specimens are
415 similar to that of specimen CC. It is evident that the present theoretical model for the beam
416 provides accurate predictions of the deflections at various locations of a DSTB for these load
417 levels (Fig. 7a). For specimen CCU (Fig. 7b), however, the model cannot provide close

418 predictions of the deflections, which is probably due to the slips between the DSTB and the
419 deck as explained earlier.
420
421 **CONCLUSIONS**
422 This paper has presented and interpreted the test results of three large-scale hybrid DSTBs
423 with headed shear studs and a DSTB/deck unit. The main parameter examined in this study
424 was the section configuration which involved the use of both rectangular and circular tubes
425 for both the outer and the inner skins. A theoretical model based on conventional section
426 analysis was also developed to predict the response of the test specimens. Based on the test
427 results and the comparisons with theoretical predictions, the following conclusions can be
428 drawn:
429 (1) Both the DSTBs and the DSTB/deck unit tested in the present study showed a very
430 ductile response.
431 (2) Both the stiffness and the load-carrying capacity of a DSTB can be substantially
432 enhanced by integrating it into a concrete deck.
433 (3) Headed shear studs can effectively eliminate the relative slips between the concrete and
434 the steel tube, leading to enhanced composite action between the two.
435 (4) The shear connection between the concrete deck and the DSTB adopted in the present
436 study was insufficient to ensure full composite action between the beam and the deck,
437 and needs to be improved.
438 (5) The predictions from the theoretical model are in reasonably close agreement with the
439 test results. Differences arise from factors not considered in the theoretical model,
440 including slips between the steel tube and the concrete and between the DSTB and the
441 deck.
442 Much further research is needed on these DSTBs and DSTB/deck units to address a

number of important issues, including the design of shear connectors and the prediction of strength and deformation considering slips between the components of the section.

ACKNOWLEDGEMENTS

The authors are grateful for the financial support provided by the Research Grants Council of the Hong Kong Special Administrate Region (PolyU 5285/10E), the National Basic Research Program of China (i.e. the 973 Program) (Project No.: 2012CB026201), and the Australian Research Council through a Discovery Early Career Researcher Award (Project ID: DE140101349) for the third author.

REFERENCES

Abdalla, H.A. (2002). "Evaluation of deflection in concrete members reinforced with fibre reinforced polymer (FRP) bars", *Composite Structures*, Vol. 56, No. 1, pp. 63-71.

Abdel-Rahman, N. and Sivakumaran, K.S. (1997). "Material properties models for analysis of cold-formed steel members", *Journal of Structural Engineering*, ASCE, Vol. 123, No. 9, pp. 1135-1143.

ACI (2008). *Building Code Requirements for Structural Concrete (ACI 318-08) and Commentary*, American Concrete Institute, 2008.

ASTM C469-02 (2002). *Standard Test Method for Static Modulus of Elasticity and Poisson's Ratio of Concrete in Compression*, American Society for Testing Materials (ASTM), West Conshohocken, PA, USA.

ASTM D3039/D3039M (2008). *Standard Test Method for Tensile Properties of Polymer Matrix Composite Materials*, American Society of Testing Materials, West Conshohocken, PA, USA.

ASTM-D7205 (2006). *Standard Test Method for Tensile Properties of Fiber Reinforced*

468 *Polymer Matrix Composite Bars*, American Society of Testing Materials, West
469 Conshohocken, PA, USA.
470 ASTM D7565/D7565M (2010). *Standard Test Method for Determining Tensile Properties of*
471 *Fiber Reinforced Polymer Matrix Composites Used for Strengthening of Civil Structures*,
472 American Society of Testing Materials (ASTM), West Conshohocken, PA, USA.
473 BS18 (1987). *Tensile Testing of Metals*, British Standards Institution, London, UK.
474 BS/EN/ISO 14555 (2006). *Welding-Arc Stud Welding of Metallic Materials*, British Standards
475 Institution, London, UK.
476 CEB-FIP (1993). *CEB-FIP Model Code 1990*, Thomas Telford, London.
477 Collings, D. (2005). *Steel Concrete Composite Bridges*, Thomas Telford, London.
478 Daniel, I.M. and Ishai, O. (2006). *Engineering Mechanics of Composite Materials*, Oxford
479 University Press, New York.
480 De Solva, C.W. (2014). *Mechanics of Materials*, CRC Press/Taylor & Francis Group, Boca
481 Raton.
482 Fam, A.Z. and Rizkalla, S.H. (2001). "Behavior of axially loaded concrete-filled circular
483 fiber-reinforced polymer tubes", *ACI Structural Journal*, Vol. 98, No. 3, pp. 280-289.
484 Gattesco, N. (1999). "Analytical modeling of nonlinear behavior of composite beams with
485 deformable connection", *Journal of Constructional Steel Research*, Vol. 52, No. 2,
486 195-218.
487 Han, L.H., Tao, Z., Liao, F.Y. and Xu, Y. (2010). "Tests on cyclic performance of
488 FRP–concrete–steel double-skin tubular columns", *Thin-Walled Structures*, Vol. 48, No.
489 6, pp. 430-439.
490 Hognestad, E. (1951). *A Study of Combined Bending and Axial Load in Reinforced Concrete*
491 *Members*, Bulletin Series No. 399 , Engineering Experiment Station, Univ. of Illinois,
492 Urbana, III.

493 Hollaway, L.C. and Teng, J.G. (2008). *Strengthening and Rehabilitation of Civil*
494 *Infrastructures Using Fibre-Reinforced Polymer (FRP) Composites*, Woodhead
495 Publishing Limited, Cambridge.
496 Idris, Y. and Ozbakkaloglu, T. (2014). "Flexural behavior of FRP-HSC-steel composite
497 beams", *Thin-Walled Structures*, Vol. 80, pp. 207-216.
498 Johnson, R.P. (1994). *Composite Structures of Steel and Concrete, Volume 1: Beams, Slabs,*
499 *Columns, and Frames for Buildings*, Blackwell Scientific Publication, Oxford.
500 Kim, H.Y., Park, K.T., Jeong, J., Lee, Y.H., Hwang, Y.K. and Kim, D. (2009). "A pultruded
501 GFRP deck panel for temporary structures", *Composite Structures*, Vol. 91, No. 1, pp.
502 20-30.
503 Li, B., Zohrevand, P. and Mirmiran, A. (2013). "Cyclic behavior of FRP concrete bridge pier
504 frames", *Journal of Bridge Engineering*, ASCE, Vol. 18, No. 5, pp. 429-438.
505 Liu, M.X. and Qian, J.R. (2007). "Moment-curvature relationships of FRP-concrete-steel
506 double-skin tubular members", *Journal of Tsinghua University (Sci&Tech)*, Vol. 47, No.
507 12, pp. 2105-2110. (in Chinese)
508 Mirmiran, A. (2003). "Stay-in-place FRP form for concrete columns", *Advances in Structural*
509 *Engineering*, Vol. 6, No. 3, pp. 321-241.
510 Nie, J.G. (2011). *Steel-Concrete Composite Bridges*, China Communications Press, Beijing.
511 (in Chinese)
512 Oehlers, D.J. and Bradford, M.A. *Elementary Behaviour of Composite Steel and Concrete*
513 *Structural Members*, Butterworth-Heinemann, Oxford.
514 Ozbakkaloglu, T. and Fanggi, B.L. (2014). "Axial compressive behavior of
515 FRP-concrete-steel double-skin tubular columns made of normal- and high-strength
516 concrete", *Journal of Composites for Construction, ASCE*, Vol. 18, No. 1,
517 04013027-1-13.

518 Ozbakkaloglu, T. and Idris, Y. (2014). “Seismic behavior of FRP-high-strength concrete-steel
519 double-skin tubular columns”, *Journal of Structural Engineering, ASCE*, Vol. 140, No. 6,
520 04014019-1-14.
521 Popovics, S. (1973). “A numerical approach to the complete stress strain curve of concrete”,
522 *Cement and Concrete Research*. Vol. 3, No. 5, pp. 583-599.
523 Qian, J.R. and Liu, M.X. (2006). “Experiment of FRP-concrete-steel double-skin tubular long
524 columns under axial compressive load”, *Concrete*, No. 9, pp. 31-34. (in Chinese)
525 Qian, J.R. and Liu, M.X. (2008a). “Experimental investigation of FRP-concrete-steel double
526 skin tubular stubs under axial compressive loading”, *Journal of Building Structures*, Vol.
527 29, No. 2, pp. 104-113. (in Chinese)
528 Qian, J.R. and Liu, M.X. (2008b). “Test of seismic behavior of FRP-concrete-steel
529 double-skin tubular columns”, *China Civil Engineering Journal*, Vol. 41, No. 3, pp. 29-36.
530 (in Chinese)
531 Qian, J.R. and Liu, M.X. (2008c). “A hysteretic model of moment-rotation relationship for
532 plastic hinge zone of FRP-concrete-steel double skin tubular columns”, *Engineering*
533 *Mechanics*, Vol. 25, No. 11, pp. 48-52. (in Chinese)
534 Teng, J.G., Chen, J.F., Smith, S.T. and Lam, L. (2002). *FRP Strengthened RC Structures*,
535 John Wiley & Sons, Ltd.
536 Teng, J.G., Yu, T. and Wong, Y.L. (2004). “Behavior of hybrid FRP-concrete-steel tubular
537 columns”, *Proceedings of the 2nd International Conference on FRP Composites in Civil*
538 *Engineering*, Taylor & Francis Ltd, Hoboken, pp. 811-818.
539 Teng, J.G., Yu, T., Wong, Y.L. and Dong, S.L. (2007). “Hybrid FRP-concrete-steel tubular
540 columns: Concept and behavior”, *Construction and Building Materials*, Vol. 21, No. 4, pp.
541 846-854.
542 Teng, J.G., Yu, T. and Fernando, D. (2012). “Strengthening of steel structures with

543 fiber-reinforced polymer composites", *Journal of Constructional Steel Research*, Vol. 78,
544 pp. 131-143.
545 Wang, Z.B. and Tao, Z. (2009). "Experimental behavior of FRP concrete steel double skin
546 tubular beams", *Industrial Construction*, Vol. 39, No. 4, pp. 5-8, 27. (in Chinese)
547 Wong, Y.L., Yu, T., Teng, J.G. and Dong, S.L. (2008). "Behavior of FRP-confined concrete in
548 annular section columns", *Composites Part B: Engineering*, Vol. 39, No. 3, pp. 451-466.
549 Yu, T., Wong, Y.L., Teng, J.G., Dong, S.L. and Lam, E.S.S. (2006). "Flexural behavior of
550 hybrid FRP-concrete-steel double-skin tubular members", *Journal of Composites for*
551 *Construction*, ASCE, Vol. 10, No. 5, pp. 443-452.
552 Yu, T. (2007). *Structural Behavior of Hybrid FRP-Concrete-Steel Double-Skin Tubular*
553 *Columns,* PhD Thesis, Department of Civil and Structural Engineering, The Hong Kong
554 Polytechnic University, Hong Kong, China.
555 Yu, T., Wong, Y.L. and Teng, J.G. (2010a). "Behavior of hybrid FRP-concrete-steel double
556 skin tubular columns subjected to eccentric compression", *Advances in Structural*
557 *Engineering*, Vol. 13, No. 5, pp. 961-974.
558 Yu, T., Teng, J.G. and Wong, Y.L. (2010b). "Stress-strain behavior of concrete in hybrid
559 FRP-concrete-steel double skin tubular columns", *Journal of Structural Engineering*,
560 ASCE, Vol. 136, No. 4, pp. 379-389.
561 Yu, T., Teng, J.G., Wong, Y.L. and Dong, S.L. (2010c). "Finite element modeling of confined
562 concrete-I: Drucker-Prager type plasticity model", *Engineering Structures*, Vol. 32, No. 3,
563 pp. 665-679.
564 Yu, T., Teng, J.G., Wong, Y.L. and Dong, S.L. (2010d). "Finite element modeling of confined
565 concrete-I: Plastic damage model", *Engineering Structures*, Vol. 32, No. 3, pp. 680-691.
566 Yu, T., Zhang, B., Cao, Y.B. and Teng, J.G. (2012). "Behavior of hybrid FRP-concrete-steel
567 double-skin tubular columns subjected to cyclic axial compression", *Thin-Walled*

568 *Structures*, Vol. 61, pp. 196-203.
569 Yu, T. and Teng, J.G. (2013). "Behaviour of hybrid FRP-concrete-steel double-skin tubular
570 columns with a square outer tube and a circular inner tube subjected to axial
571 compression", *Journal of Composites for Construction,* ASCE, Vol. 17, No. 2, pp.
572 271-279.
573 Zhang, B., Teng, J.G. and Yu, T. (2015). "Experimental behavior of hybrid
574 FRP-concrete-steel double-skin tubular columns under combined axial compression and
575 cyclic lateral loading", *Engineering Structures*, Vol. 99, pp. 214–231.
576

LIST OF TABLES:

LIST OF FIGURES:

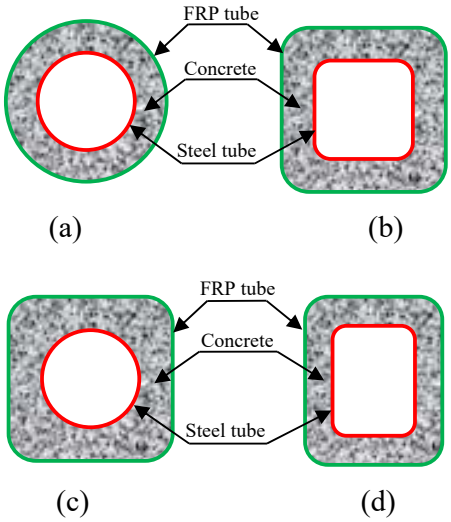

Fig. 1. Typical cross-sections of double-skin tubular columns

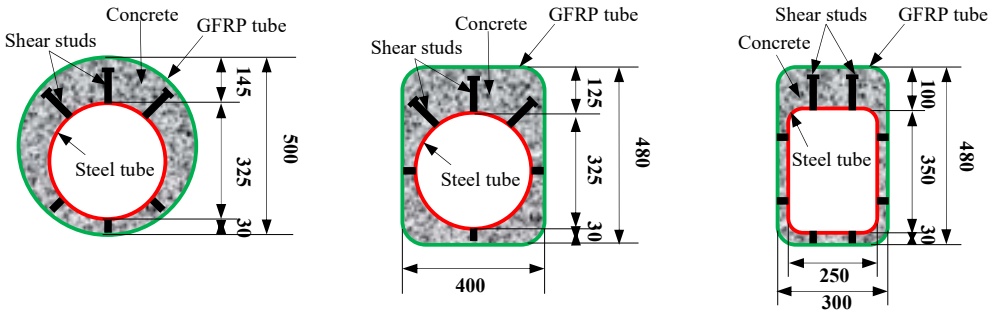

(a) Specimen CC (b) Specimen RC (c) Specimen RR

(Dimensions in mm)

Fig. 2. Cross-sections of double-skin tubular beam specimens

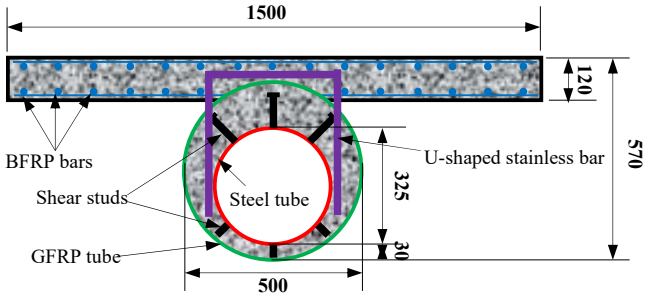

(Dimensions in mm)

Fig. 3. Cross-section of hybrid DSTB/deck unit (specimen CCU)

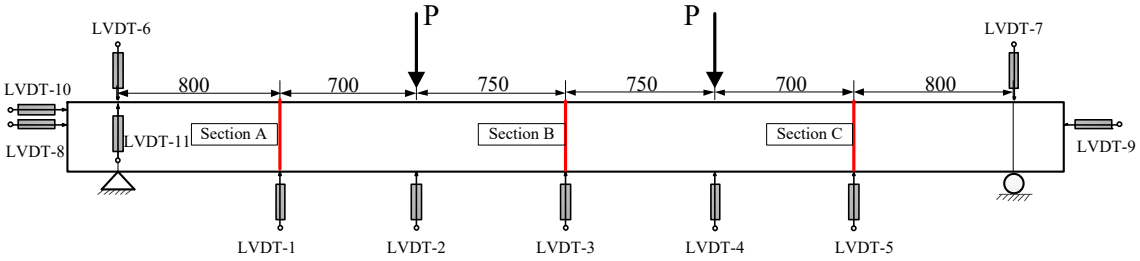

(a) Four-point bending tests (specimens CC, RC and RR)

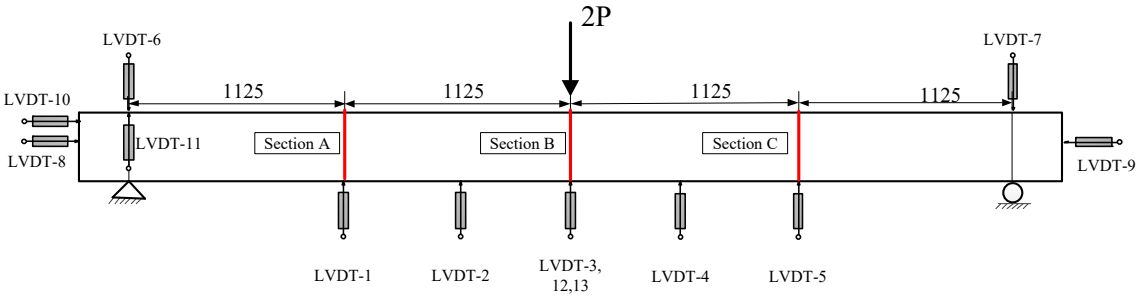

(b) Three-point bending test (specimen CCU)

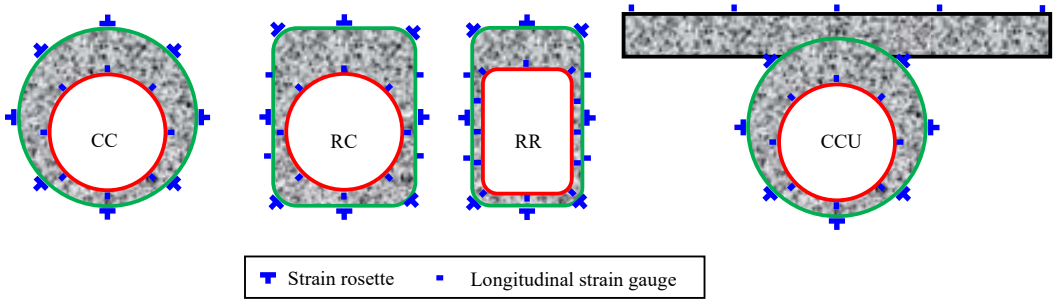

(c) Layout of strain gauges at sections A to C

(Dimensions in mm)

Fig. 4. Test set-up and instrumentation

(a) Specimen CC (b) Specimen CCU

Fig. 5. Tests in progress

(a) Specimen CC

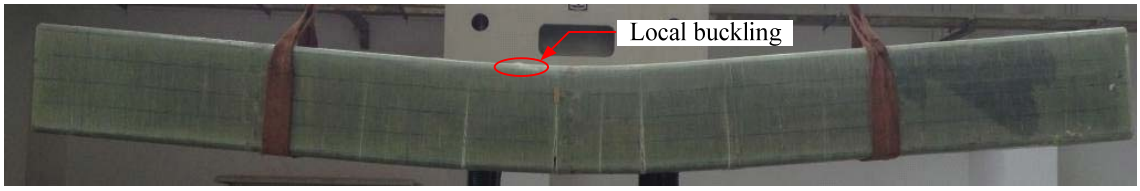

(b) Specimen RC

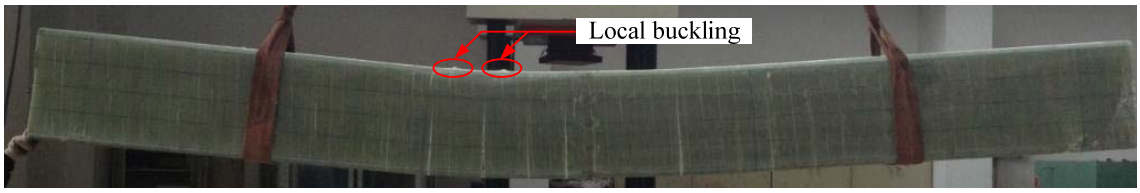

(c) Specimen RR

(d) Specimen CCU

Fig. 6. Specimens after test

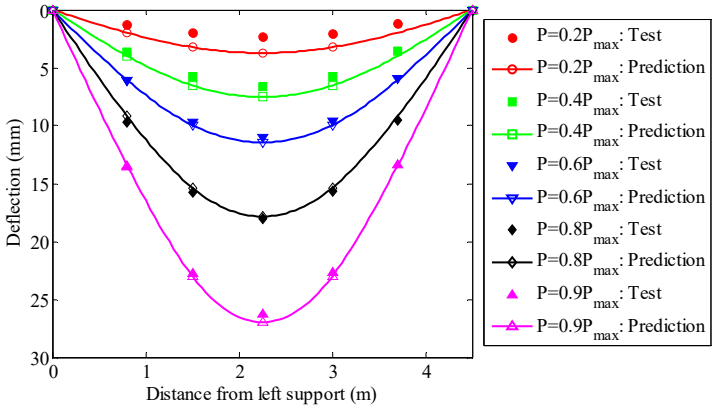

(a) Specimen CC

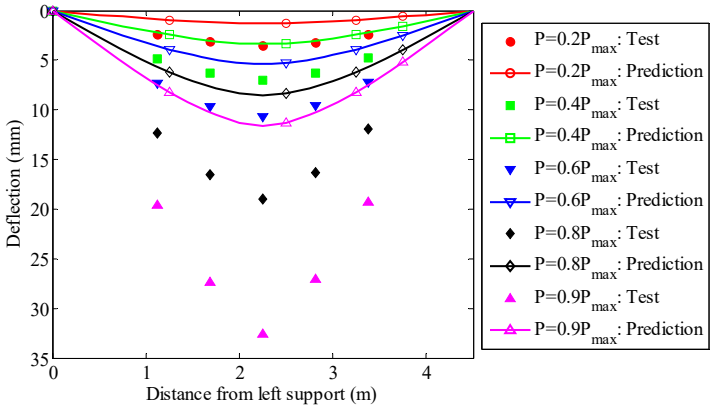

(b) Specimen CCU

Fig. 7. Deflected shapes of test specimens

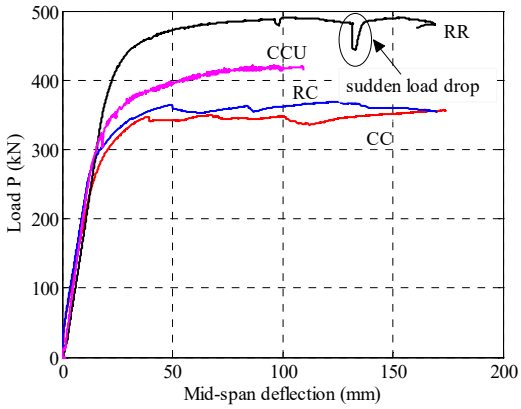

Fig. 8. Load versus mid-span deflection

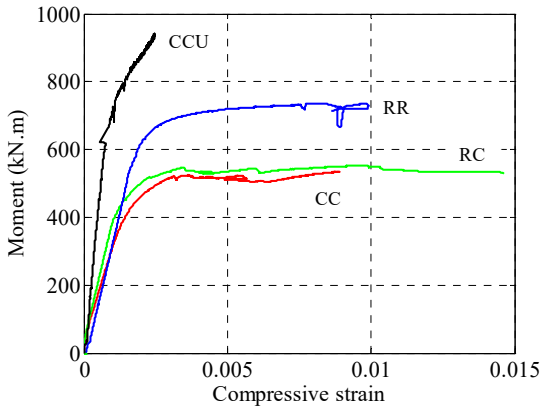

Fig. 9. Moment versus strain at extreme compression fiber

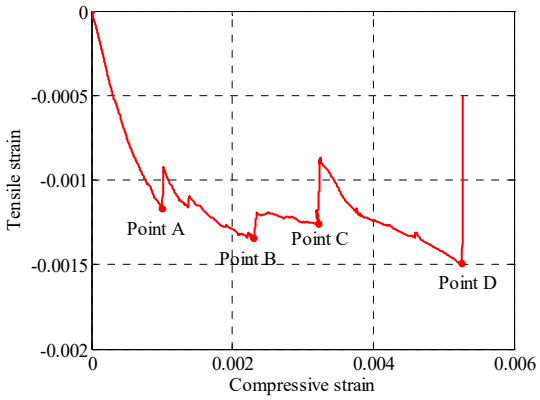

Fig. 10. Compressive-tensile strain curves of specimen CC

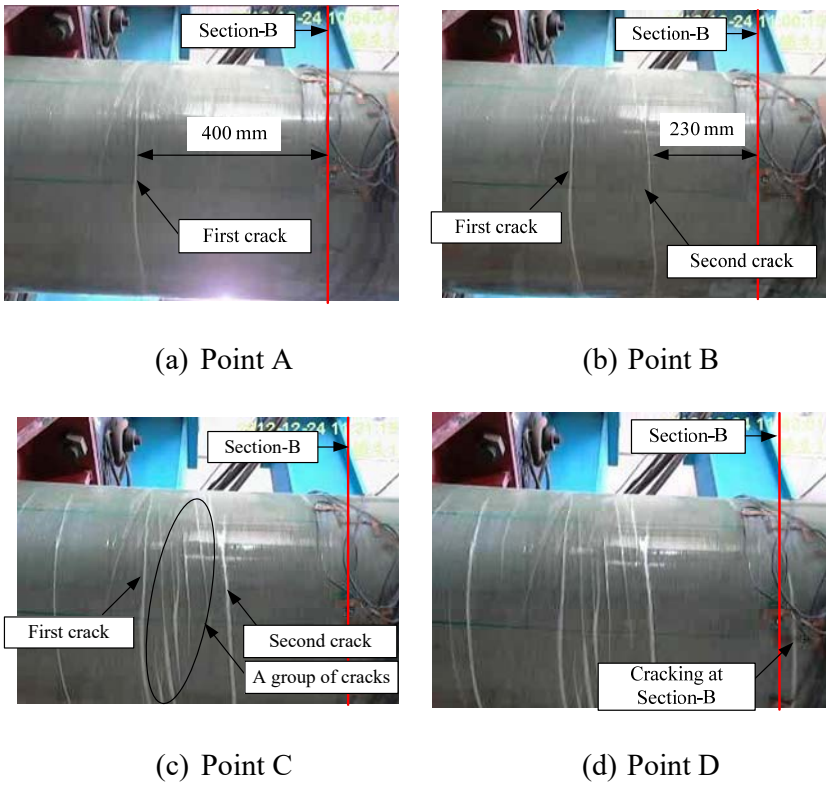

(a) Point A (b) Point B

(c) Point C (d) Point D

Fig. 11. Development of cracks on FRP tube in specimen CC

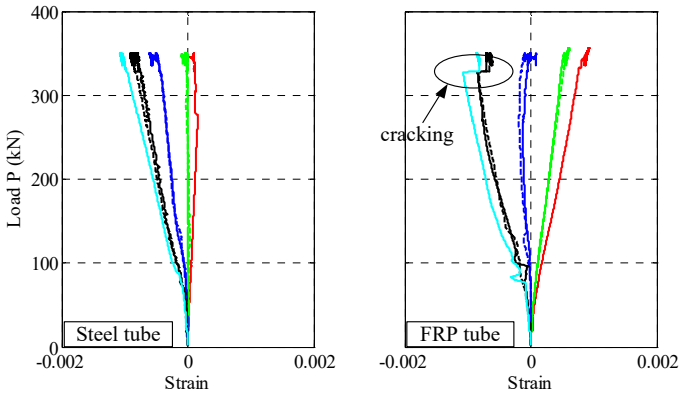

(a) Specimen CC

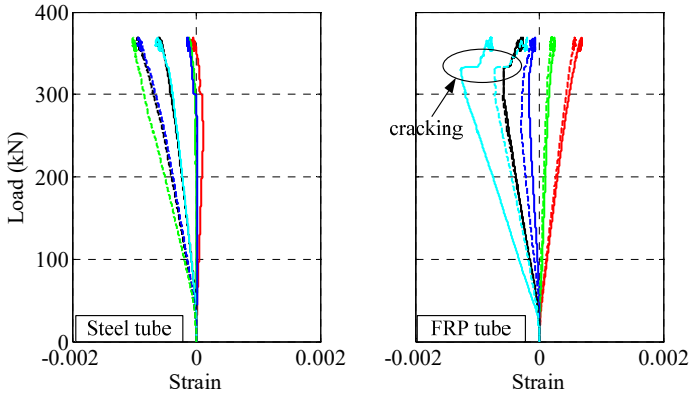

(b) Specimen RC

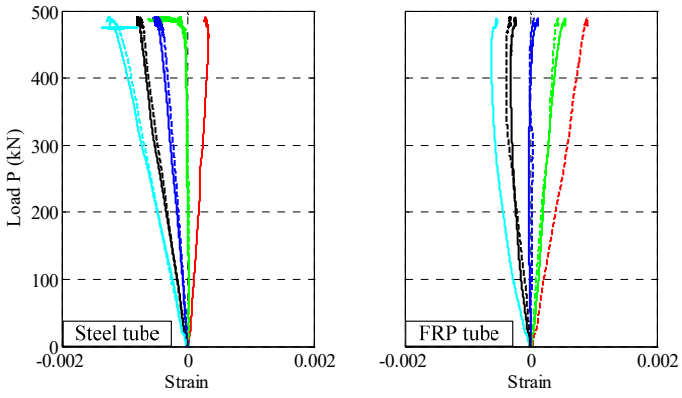

(c) Specimen RR

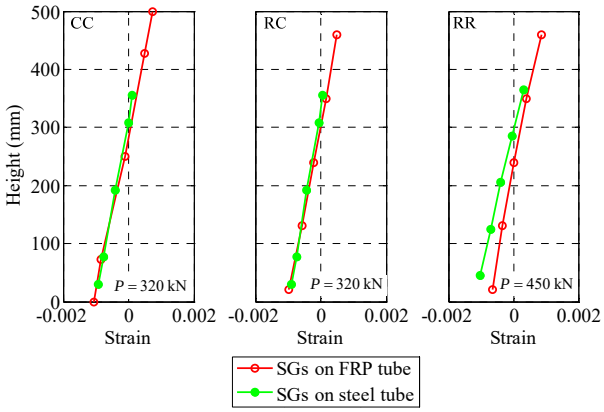

(d) Strain distribution down the height

Fig. 12. Development of longitudinal strains at section A

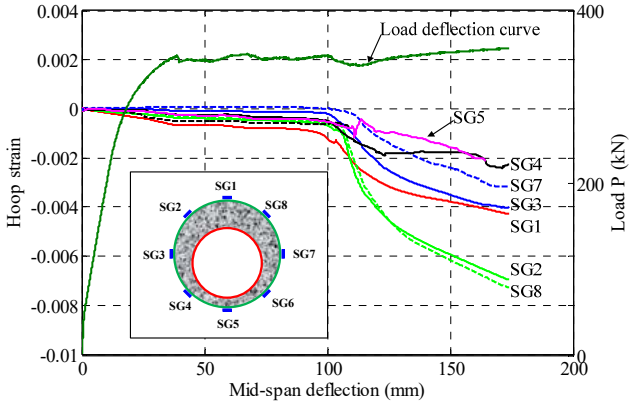

(a) Specimen CC

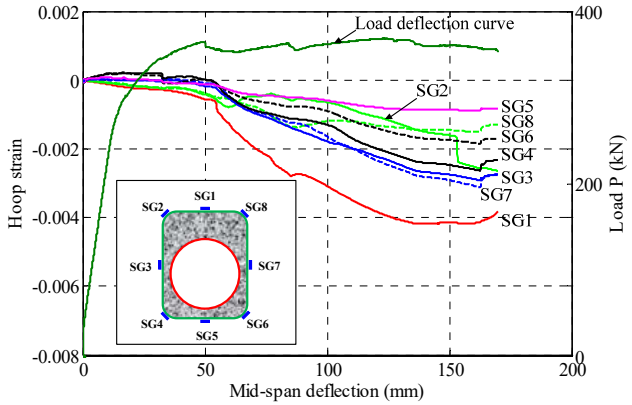

(b) Specimen RC

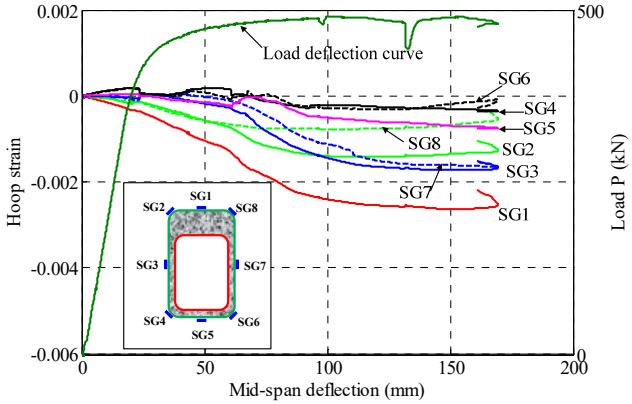

(c) Specimen RR

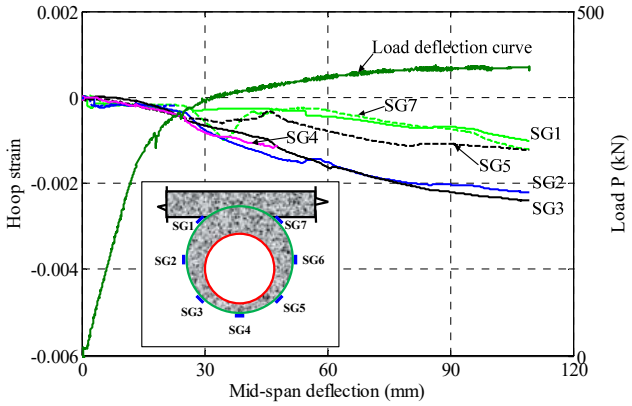

(d) Specimen CCU

Fig. 13. Development of hoop strains on FRP tube at section B

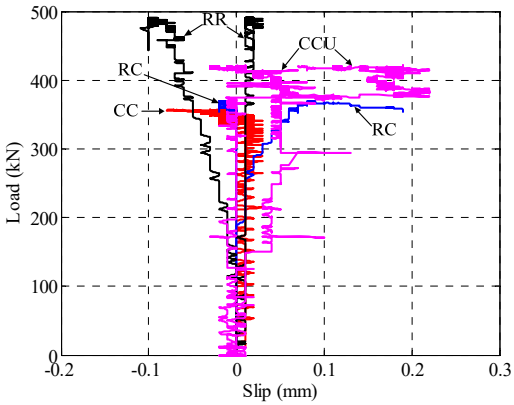

Fig. 14. Slips between steel tube and concrete

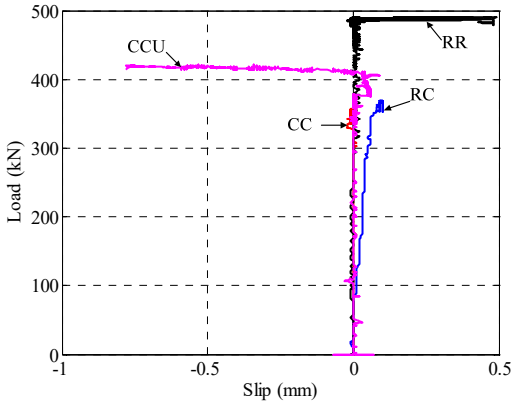

Fig. 15. Slips between FRP tube and concrete

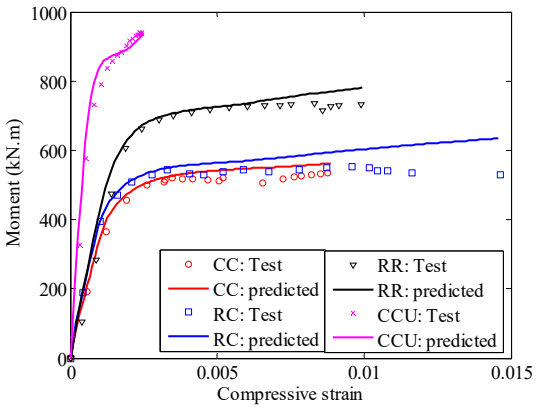

Fig 16. Moment-strain curves: predictions versus test results

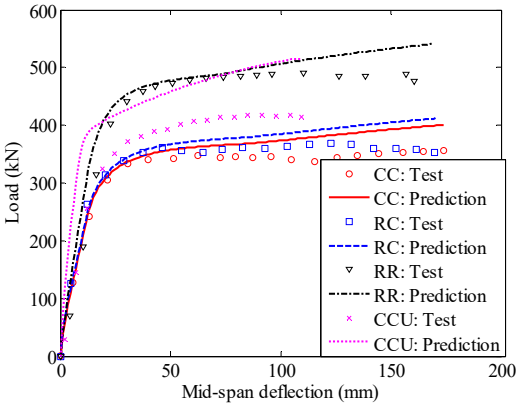

Fig. 17. Load-deflection curves: predictions versus test results

Table 1. Mechanical properties of steel/BFRP components

Material	Elastic modulus (GPa)	Yield strength (MPa)	Tensile strength (MPa)
Circular steel tube	200	322	473
Rectangular steel tube*	208(225)	313	464(539)
Stainless steel bar	198	——	699
Shear stud	196	——	439
BFRP bar	40.8	——	690

*Note: The values outside the parentheses were obtained from the web coupon tests while those in the parentheses were obtained from the corner coupon tests.

Table 2. Mechanical properties of fibre and resin for FRP tubes

Material	Tensile strength (MPa)	Tensile Modulus (GPa)	Rupture strain (%)
E-glass fiber	1970	78.8	——
Vinyl ester	95	3.6	6.1